



Article

Syntheses and Structures of Novel λ^3, λ^3 -Phosphanylalumanes Fully Bearing Carbon Substituents and Their Substituent Effects

Tatsuya Yanagisawa ¹, Yoshiyuki Mizuhata ^{1,2,*} and Norihiro Tokitoh ^{1,2,*}

¹ Institute for Chemical Research, Kyoto University, Gokasho, Uji, Kyoto 611-0011, Japan; yanagisawa@boc.kuicr.kyoto-u.ac.jp

² Integrated Research Consortium on Chemical Sciences, Uji, Kyoto 611-0011, Japan

* Correspondence: mizu@boc.kuicr.kyoto-u.ac.jp (Y.M.); tokitoh@boc.kuicr.kyoto-u.ac.jp (N.T.); Tel.: +81-774-38-3203 (Y.M.); +81-774-38-3200 (N.T.)

Received: 16 October 2019; Accepted: 5 November 2019; Published: 7 November 2019



Abstract: The novel phosphanylalumanes, Al–P single-bond species, fully bearing carbon protecting groups on aluminum and phosphorus atoms, are synthesized by the reactions of aluminum monohalides [(*t*-Bu)₂AlBr and (C₆F₅)₂AlCl·0.5(toluene)] with Mes₂PLi. Regarding the *t*-Bu system, λ^3, λ^3 -phosphanylalumane is obtained. Concerning the C₆F₅ system, on the other hand, the corresponding LiCl complex, λ^4, λ^4 -phosphanylalumane, is obtained. The Al–P bond lengths of C₆F₅-substituted λ^3, λ^4 -, and λ^4, λ^4 -derivatives are much shorter than those of the reported λ^3, λ^4 -phosphanylalumane derivatives and comparable to that observed for the previously reported λ^3, λ^3 -phosphanylalumanes. Theoretical calculations reveal that the binding of the C₆F₅ groups to Al results in a large contribution of Al and a large *s*-character in the Al–P bond of phosphanylalumanes. Considering *t*-Bu-substituted phosphanylalumanes, the Al–P bond lengths reflect the coordination number of Al, showing a longer Al–P bond length in the case of λ^4 -Al as compared with that of λ^3 -Al. Combining the structural, spectroscopic, and theoretical results, the *t*-Bu-substituted λ^3, λ^3 -phosphanylalumane has well separated vacant p orbital and lone pairs, which is suitable for reactivity studies.

Keywords: phosphanylalumanes; aluminum; phosphorus; Al–P bond

1. Introduction

The bonding between group 13 (E) and group 15 (Pn) elements formulated as R₂E–PnR₂ have attracted much attention due to their relationship, including the vacant p orbital on E and the lone-pair electrons on Pn. Aminoboranes (R₂B–NR₂), for example, have an enormous number of researches describing their [–]B=N⁺ polar double-bond character [1]. To contrast, the heavier analogues, λ^3, λ^3 -phosphanylalumanes (R₂Al–PR₂), decrease the π -type interaction between the E and Pn atoms compared to those of aminoboranes [2–4] and phosphanylboranes [5,6] due to the longer E–Pn σ -bond. These aspects can afford a characteristic reactivity reflecting the adjacent but separated Lewis acids and bases, similar to the synergetic interactions of the Lewis acid and Lewis base of frustrated Lewis pairs (FLPs) toward small-molecules [7–10].

The physical properties and reactivity of λ^3, λ^3 -phosphanylalumanes, however, hardly have been clarified so far. The main reason is that there are few synthetic examples due to the difficulty of protecting the vacant 3p(Al) orbital [11–13]. Most of λ^3, λ^3 -phosphanylalumanes have been synthesized by the salt elimination reactions reported by Power [14], Nöth and Paine [15,16], and our group [17] (Figure 1a). Multi-nuclear phosphanylalumane derivatives are also known. When there are reactive substituents (H or a halogen atom) on P or Al moiety, another aluminum or phosphorus reagents react

to give a λ^3, λ^3 -diphosphanyl- λ^3 -alumane [16] and λ^3 -phosphanyl- λ^3, λ^3 -dialumane [17], respectively (Figure 1b). A cyclic λ^3, λ^3 -phosphanylalumane ($\text{Mes}^*\text{Al-PPh}$)₃ is synthesized by a dehydrogenation reaction, which is thought to be the trimerization of an Al-P double-bond compound (Figure 1c) [18]. Regarding each case, at least one substituent on an Al or P atom is a heteroatom (non-carbon atom) substituent, which will affect the nature of the Al-P bond. The Lewis acidity of aluminum, for example, is greatly impaired by mesomeric effect between the vacant 3p(Al) orbital and the one pair on aluminum-bound substituents [19,20]. Electropositive substituents (SiPh_3 , SiMe_3 , and SnMe_3) attached to the P atom also may alter the nature of the Al-P bond. Therefore, the synthesis and elucidation of the reactivity of unperturbed, all-carbon-substituted λ^3, λ^3 -phosphanylalumanes might be a new challenge.

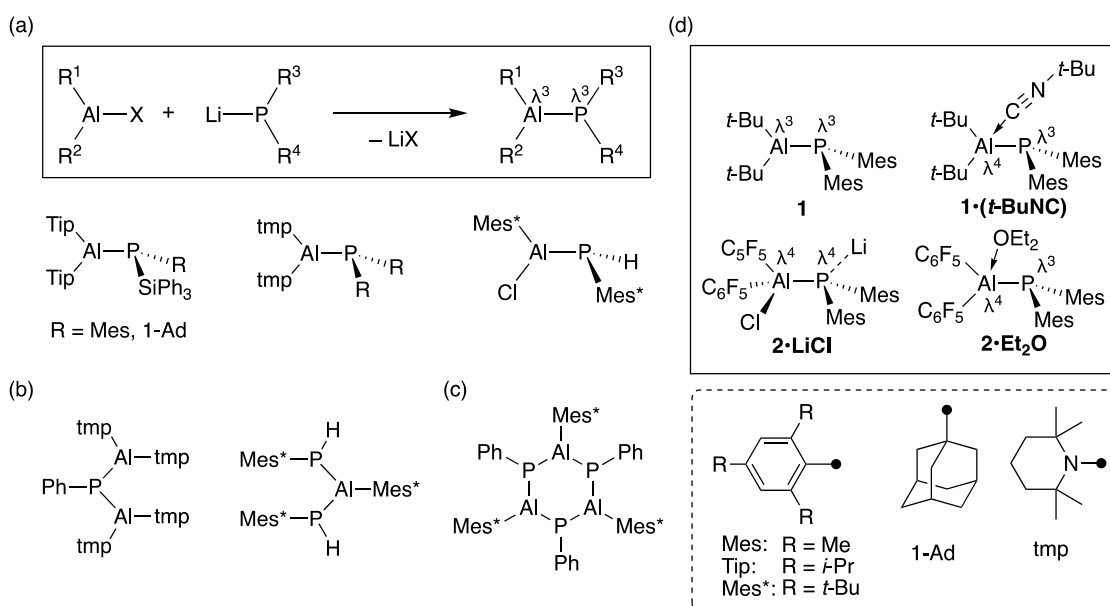
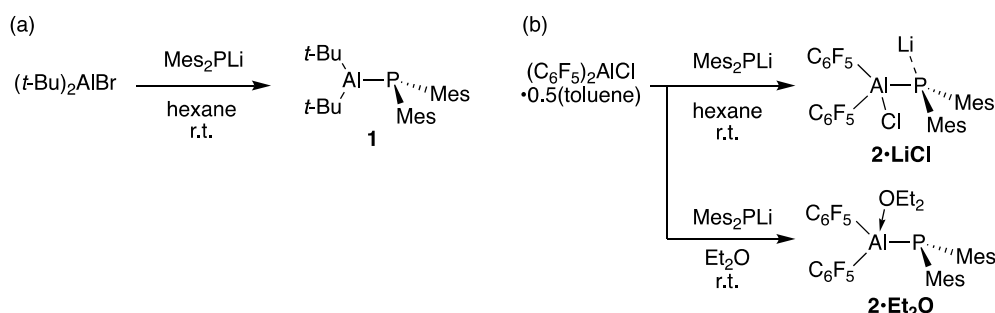


Figure 1. Known phosphanylalumanes. (a) Synthetic strategy of λ^3, λ^3 -phosphanylalumanes. (b) λ^3 -Phosphanyl- λ^3, λ^3 -dialumane and λ^3, λ^3 -diphosphanyl- λ^3 -alumane. (c) Cyclic λ^3, λ^3 -phosphanylalumane. (d) Phosphanylalumane derivatives with carbon protecting groups on Al and P atoms described in this study.

Here, we report the synthesis of λ^3, λ^3 -phosphanylalumanes which are substituted fully by carbon protecting groups on the aluminum and phosphorus atoms. To understand the substituent effect on the aluminum, we chose *t*-Bu and C_6F_5 groups (Figure 1d).

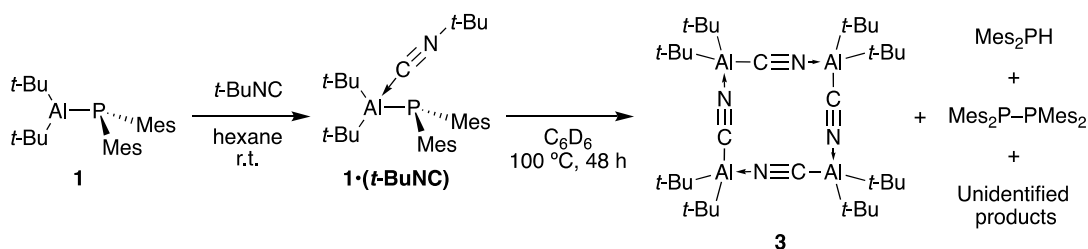
2. Results and Discussion

The reaction of $(t\text{-Bu})_2\text{AlBr}$ [21] with Mes_2PLi [22] afforded a λ^3, λ^3 -phosphanylalumane **1** quantitatively, judged by ^{31}P NMR spectroscopy (Scheme 1a). Conversely, the use of $(\text{C}_6\text{F}_5)_2\text{AlCl} \cdot 0.5(\text{toluene})$ [23] as an aluminum source in a hexane solution afforded an LiCl complex, λ^4, λ^4 -phosphanylalumane **2**·LiCl, in a 54% yield (Scheme 1b). We expected that the use of $(\text{C}_6\text{F}_5)_2\text{AlBr}$ [23] would render a more effective salt elimination but the corresponding LiBr complex (**2**·LiBr) was detected by NMR spectroscopy. No salt elimination in the case of the C_6F_5 substituent suggested the higher Lewis acidity of the aluminum atom on $(\text{C}_6\text{F}_5)_2\text{Al}$ -moiety as compared with that on the $t\text{-Bu}_2\text{Al}$ moiety. The attempts of LiCl elimination from **2**·LiCl by heating or the addition of silver tetrafluoroborate were not successful. Although the reaction of $(\text{C}_6\text{F}_5)_2\text{AlCl} \cdot 0.5(\text{toluene})$ in an Et_2O solution, rather than hexane afforded a complicated mixture, recrystallization from which gave an etherate **2**·Et₂O in a 38% yield. The addition of Et_2O to **2**·LiCl led to the formation of compound **2**·Et₂O, which was evidenced in the mixture of $(\text{C}_6\text{F}_5)_2\text{AlCl} \cdot 0.5(\text{toluene})$ with Mes_2PLi in Et_2O . These results suggest that **2**·LiCl was formed at the initial stage in both conditions and the partial decomposition occurred via Et_2O in addition to the formation of **2**·Et₂O.



Scheme 1. Synthesis of phosphanylalumane derivatives bearing (a) *t*-Bu and (b) C_6F_5 groups on Al atoms.

Subsequently, the coordination of Lewis bases was examined to explore the Lewis acidity of λ^3, λ^3 -phosphanylalumane **1**. Although **1** did not react with carbon monoxide upon heating to 70°C , the reaction of **1** with *t*-butyl isocyanide at room temperature gave the Lewis base-coordinated λ^3, λ^4 -complex **1·(t-BuNC)** quantitatively (Scheme 2). Heating of a C_6D_6 solution of **1·(t-BuNC)** with the aim of further isomerization and coupling of isocyanides [24–26] produced a mixture containing a **1**, **1·(t-BuNC)**, Mes_2PH , and $\text{Mes}_2\text{P-PMes}_2$ as judged by the ^{31}P NMR spectrum. The recrystallization from the mixture afforded a trace amount of single crystals of bis(*t*-butyl)aluminum cyanide tetramer **3** [27], as determined by NMR measurements and X-ray crystallography. The elimination of the *t*-Bu group from *t*-BuNC to form diorganylaluminum cyanides $(\text{R}_2\text{AlCN})_n$ also has been observed in the reaction of the Al–Al bond compound with *t*-BuNC [24]. Heating at elevated temperatures promotes desorption of the $(t\text{-Bu})_2(t\text{-BuNC})\text{Al-}$ and $\text{Mes}_2\text{P-}$ moieties to give **3**, Mes_2PH , and $\text{Mes}_2\text{P-PMes}_2$.



Scheme 2. Lewis base (*t*-BuNC) coordination to **1** and thermal reaction of **1·(t-BuNC)**.

Structures of all new phosphanylalumane derivatives **1**, **1·(t-BuNC)**, **2·LiCl**, and **2·Et}_2\text{O}** were determined finally by X-ray crystallography, and the results showed good agreement with the optimized structures calculated at the B3LYP-D3/6-31G(d) level. These structures are depicted in Figure 2 and the structural features of these compounds are summarized in Table 1. Particularly, **2·LiCl** had a one-dimensional infinite chain structure with continuous $[-\text{Cl}-\text{Al}-\text{P}-\text{Li}-]$ parts. One Li atom of **2·LiCl** was coordinated by P and two F atoms of the C_6F_5 groups. Concerning complex **2·LiCl**, its anion part (**2Cl**[−]) without Li^+ , also was used for the calculations. There was almost no structural difference between the optimized structures, **2·LiCl** and **2Cl**[−]. Lewis base-free λ^3, λ^3 -phosphanylalumane **2** could not be obtained experimentally, but the optimized structural parameters of **2** also are described for the comparison.

The sum of the bond angles around the P atom (ΣP) of these compounds are $325\text{--}328^\circ$, indicating the pyramidalized structures of the phosphorus moieties despite the different coordination. Conversely, the sum of the bond angles around the Al atom (ΣAl) reflected the environment on the coordination of Al atoms. λ^3, λ^3 -Phosphanylalumane **1** retained the planar structure with the Al center ($\Sigma\text{Al} = 357^\circ$). The λ^4 -Al moieties of **1·(t-BuNC)** and **2·Et}_2\text{O}** were pyramidalized slightly ($\Sigma\text{Al} = 354^\circ$ and 347° , respectively), reflecting the weak coordination of isocyanide and diethyl ether to the λ^3 -Al atoms.

To contrast, the λ^4 -Al center of **2**·LiCl was pyramidalized extremely ($\Sigma\text{Al} = 319^\circ$), suggesting its strong Al–Cl covalent bond.

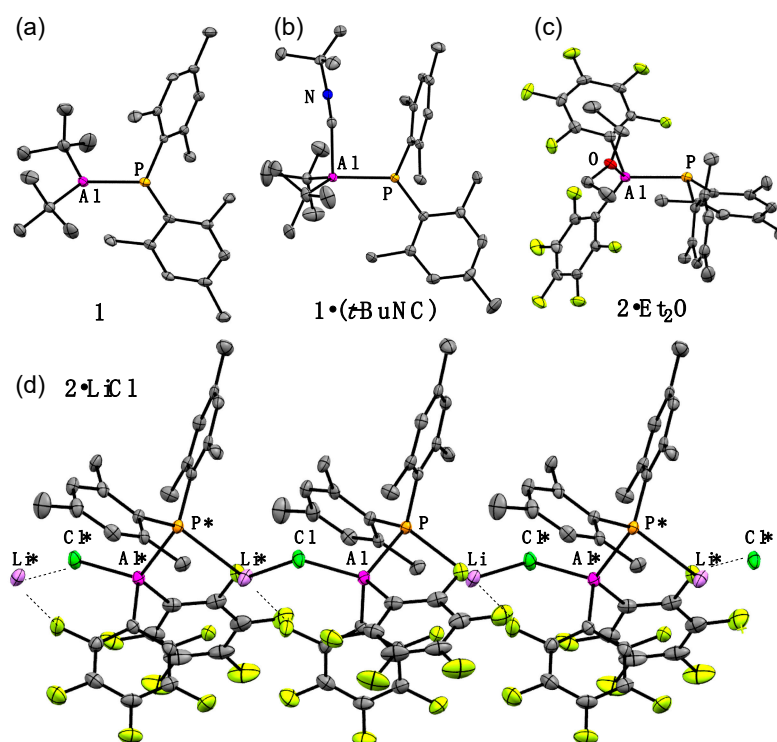


Figure 2. Structures of (a) **1**, (b) **1**·(*t*-BuNC), (c) **2**·Et₂O, and (d) **2**·LiCl (thermal ellipsoids at the 50% probability level). One of the two crystallographically independent molecules of **1** is shown here. Hydrogen atoms and solvent molecules are omitted for clarity. Color code: Al, magenta; C, gray; Cl, green; F, yellow; Li, purple; N, blue; O, red; P, orange.

Table 1. Structural parameters of **1**, **1**·(*t*-BuNC), **2**, **2**·LiCl, **2**Cl[−], and **2**·Et₂O.

Compound	Al–P/Å	$\Sigma\text{Al}/\text{deg}$	$\Sigma\text{P}/\text{deg}$	$\delta(^{31}\text{P})/\text{ppm}$
1 (obsd.) ¹	2.343(1)/2.347(1)	357/356	325/323	−111.7
1 (calcd.) ²	2.348	357	325	−
1 ·(<i>t</i> -BuNC) (obsd.)	2.4120(6)	354	328	−96.7
1 ·(<i>t</i> -BuNC) (calcd.) ²	2.435	355	330	−
2 (calcd.) ²	2.322	357	312	−
2 ·LiCl (obsd.)	2.348(1)	319	327	−89.7
2 ·LiCl (calcd.) ²	2.434	312	327	−
2 Cl [−] (calcd.) ²	2.411	321	321	−
2 ·Et ₂ O (obsd.)	2.359(2)	347	326	−104.8
2 ·Et ₂ O (calcd.) ²	2.364	352	320	−

¹ Two independent molecules. ² Calculated at the B3LYP-D3/6-31G(d) level.

The viewpoint of the Al–P bond lengths brought us the effect of electronic situations on the Al atom. The Al–P bond lengths of **1** (2.343(1) and 2.347(1) Å for two independent molecules) were comparable to that of the reported λ^3, λ^3 -phosphanalumanes (Tip₂Al–P(SiPh₃)Mes: 2.342(2) Å) [14] or the Al₃P₃ six-membered-ring compound ((Mes*Al–PPh)₃: 2.323(3)–2.336(3) Å) [18]. The coordination of *t*-BuNC to the λ^3 -Al center resulted in the large elongation of the Al–P bond (**1**·(*t*-BuNC): 2.4120(6) Å). Alternately, the Al–P bond lengths of C₆F₅-substituted λ^4 -Al-derivatives, **2**·LiCl (2.348(1) Å) and **2**·Et₂O (2.359(2) Å), were close to those of λ^3, λ^3 -phosphanalumanes **1** and much shorter than those of **1**·(*t*-BuNC) and the reported phosphanyl- λ^4 -alumanes, ((*t*-Bu)₂Al–P(SiPh₃)Tip·Et₂O: 2.416(3) Å) [12] and (Bbp(Br)Al–P(H)Mes·LiBr(Et₂O)₂: 2.4055(7) Å) [13]. Considering the observations

above, the C_6F_5 -substituted λ^3 -Al-derivative **2** is expected to have a quite short Al–P bond. However, the calculated Al–P bond length of **2** almost was similar to or slightly shorter than that of **1** (**1**: 2.348 Å vs. **2**: 2.322 Å). These results indicated that the C_6F_5 groups greatly affected the Al–P bond regardless of the coordination number to the Al center, the reasons of which will be discussed later.

The observed structural features reflect the NMR spectroscopic results. The ^{31}P NMR spectra for λ^3, λ^3 -phosphanylaluminum **1** displayed a resonance at $\delta = -111.7$ ppm that is the most upfield among those of the synthesized phosphanylaluminum derivatives (**1**·(*t*-BuNC): -96.7 ppm, **2**·Et₂O: -104.8 ppm, and **2**·LiCl: -89.7 ppm). Additionally, these ^{31}P NMR signals are in much lower magnetic fields than those of $tmp_2Al-P(SiMe_3)_2$ and $tmp_2Al-P(SnMe_3)_2$ ($\delta = -238$ and -282 ppm, respectively) [16] having an electron-donating substituent on λ^3 -P atoms, while being more upfield than that of $tmp_2Al-PPh_2$ ($\delta = -42.9$ ppm) [15]. These values indicate a sufficiently electron-rich environment for the λ^3 -P atom with carbon protecting groups in **1**. Conversely, the ^{27}Al NMR spectra for **1** showed a single broad resonance at $\delta = 261$ ppm. This value is upfield as compared with those of the reported λ^3, λ^3 -phosphanylaluminas, i.e., $tmp_2Al-PPh_2$ ($\delta = 110$ ppm) [15] and $tmp_2Al-P(SiMe_3)_2$ ($\delta = 78$ ppm) [16].

The photophysical behavior of λ^3, λ^3 -phosphanylaluminum **1** has been investigated for the first time to obtain further insight for the character of a λ^3 -Al moiety. UV–vis absorption spectrum of **1** is shown in Figure 3 with the simulated spectrum of **1** derived from time-dependent density functional theory (TD-DFT) calculations at the B3LYP-D3/6-311+G(d,p)//B3LYP-D3/6-31G(d) level of theory, which reproduced the spectrum observed experimentally. The shoulder absorption at ~ 350 nm should be assigned to the n–p transition from the highest occupied molecular orbital (HOMO) to the lowest unoccupied molecular orbital (LUMO), which corresponds to the electron transition of a lone pair of P to a vacant p orbital of Al (Figure 3a; (A)). The absorption maximum at 314 nm ($\epsilon 5.2 \times 10^3$) was assigned to the n– π^* transition from the HOMO to the LUMO+1, which corresponds to the electron transition of a lone pair of P to π^* orbitals of the Mes_2P moiety (Figure 3a; (B)). Combining the experimental and theoretical results, the vacant p orbital of λ^3, λ^3 -phosphanylaluminum **1** greatly contributes to the absorption behavior. Particularly, the λ^3, λ^3 -phosphanylaluminas with the unperturbed vacant p orbital of Al exhibit a yellow color (**1** and $Tip_2Al-P(SiPh_3)Mes$ (no UV–vis absorption spectrum) [14]), whereas the λ^3, λ^3 -phosphanylaluminas with the filled p orbital of Al by the Al-bound substituents are colorless ($tmp_2Al-P(SiMe_3)_2$ [16] and $Mes^*(Cl)Al-P(H)Mes^*$ [17]).

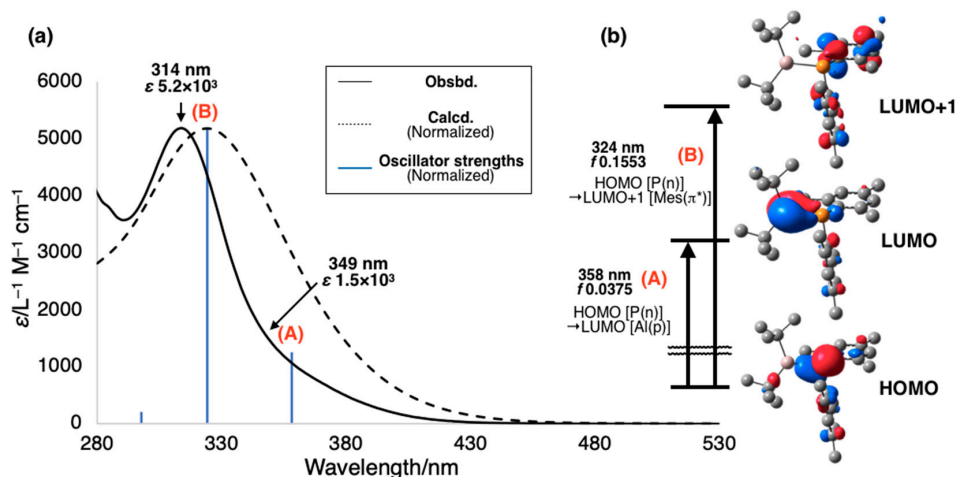


Figure 3. (a) Observed (in hexane at 298 K) and simulated (derived from TD-DFT calculations at the B3LYP-D3/6-311+G(d,p)//B3LYP-D3/6-31G(d) level of theory) UV–Vis spectrum for **1**, whereby the calculated oscillator strengths are shown as blue vertical lines. (b) Electronic transitions corresponding to the absorptions (A) and (B). Hydrogen atoms are omitted for clarity. Color code: Al, pink; C, light gray; P, orange.

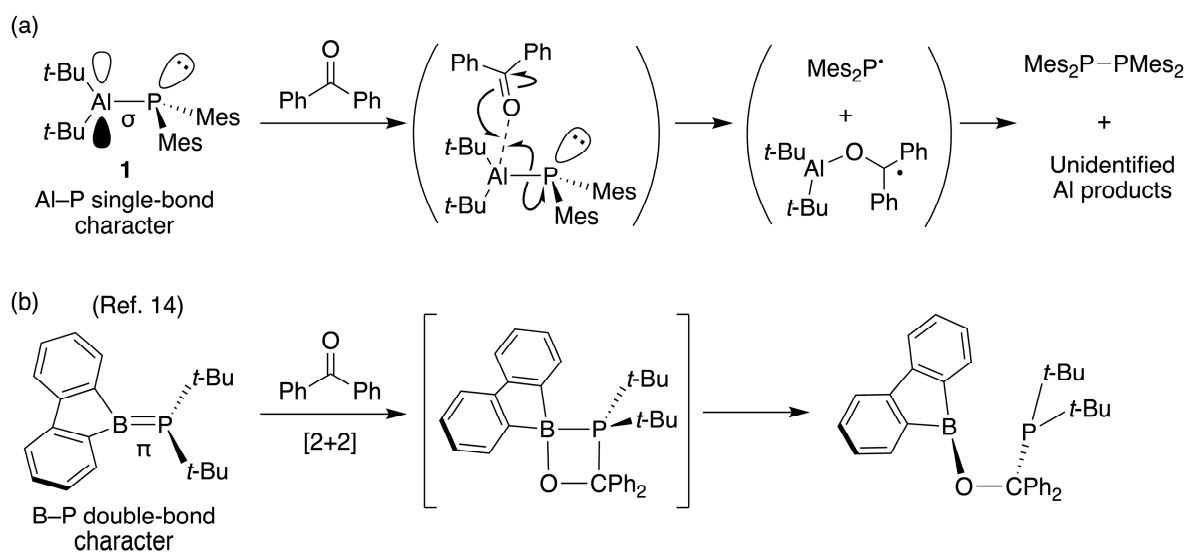
The consideration of the Al–P bonds for the newly synthesized phosphanylalumane derivatives was further deepened by the natural bond orbital (NBO) analysis, as summarized in Table 2. The π -type NBOs involving the p(Al) orbitals were not found in **1** and **2**. The natural population analysis (NPA) charge on Al of **1** (1.760) is the most positive among these phosphanylalumane derivatives, indicating the substantial retention of the vacant 3p(Al) orbital. The NBO corresponding to the σ (Al–P) bond in **1** consisted mainly of 3s(Al) and 3p(P) orbitals and was polarized toward an λ^3 -P moiety. The coordination of *t*-BuNC to λ^3 -Al increases the contribution of the hybridization of Al in σ (Al–P) bonds (**1**: 18% Al vs. **1**·(*t*-BuNC): 21% Al) and decreases the *s*-character of Al (**1**: Al sp^{1.7} vs. **1**·(*t*-BuNC): Al sp^{2.6}), as well as the experimentally observed elongation of an Al–P bond. Substitution of *t*-Bu groups with C₆F₅ groups resulted in the higher *s*-character of the Al atom in **2** than that of **1**. These are due to the use of more *p*-character in the bonding to the aryl group than that to the alkyl group and of the large inductive effect of the F atoms. This result was supported by the large Al contribution of **2**, **2Cl**[−], and **2LiCl** compared to **1** in σ (Al–P) bonds (**1**: 18% Al vs. **2**, **2Cl**[−], and **2LiCl**: 23–26% Al) and the large *s*-character of Al (**1**: Al sp^{1.7} vs. **2**, **2Cl**[−], and **2LiCl**: Al sp^{0.6–0.9}), as well as the short Al–P bond lengths independent of the coordination-number change in the Al moieties of C₆F₅-derivatives. Additionally, compound **2** showed a WBI value greater than that of **1** (**1**: 0.6595 vs. **2**: 0.7781) corresponding to the short Al–P bonds of **2LiCl** and **2Et₂O**, but the NPA charge of the λ^3 -Al moiety of **2** was less than that of **1** (**1**: 1.760 vs. **2**: 1.537). These results of the theoretical calculations suggest that compound **1** is a suitable λ^3, λ^3 -phosphanylalumane for reactivity studies.

Table 2. Summary of NBO analysis.

Compounds	WBI ¹	Q _{Al} ²	Q _P ²	NBO ³ σ (Al–P)
1	0.6595	1.760	0.07097	18.2% Al sp ^{1.71} + 81.8% P sp ^{4.19} (1.87e)
1 ·(<i>t</i> -BuNC)	0.6859	1.537	0.1445	21.0% Al sp ^{2.57} + 79.0% P sp ^{3.92} (1.88e)
2	0.7781	1.537	1.642	26.4% Al sp ^{1.16} + 73.6% P sp ^{4.93} (1.93e)
2Cl [−]	0.6843	1.446	0.1612	24.4% Al sp ^{0.83} + 75.6% P sp ^{4.18} (1.92e)
2LiCl	0.6346	1.446	−0.00425	22.5% Al sp ^{0.92} + 77.5% P sp ^{3.27} (1.93e)
2Et₂O	0.7196	1.642	0.1148	25.0% Al sp ^{0.62} + 75.0% P sp ^{3.74} (1.93e)

¹ Wiberg bond indices. ² Q_E: Natural population analysis (NPA) charge on E. ³ Natural bond orbital.

The singularity of the Al–P single-bond in **1** among the bonds between the group 13 and group 15 elements also was experimentally investigated. Treatment of **1** with benzophenone at room temperature rapidly gave Mes₂P–PMes₂ quantitatively, as judged by the ³¹P NMR spectrum (Scheme 3a), but the corresponding Al moiety was not identified. This result implied that the coordination of benzophenone to Al promoted homolysis to produce an Mes₂P radical and the corresponding radical containing an Al moiety, respectively. It was difficult to clear the radical mechanism by using (2,2,6,6-tetramethylpiperidin-1-yl)oxyl (TEMPO) because compound **1** reacted with TEMPO to give a mixture containing Mes₂P–PMes₂ and Mes₂PH. Conversely, a B–P bond compound with λ^3 -B and P centers, phosphaboradibenzofulvene, gave a [2+2]-cycloaddition product when treated with benzophenone (Scheme 3b) [28]. Contrary to the large contribution of the B–P π -bond character in a phosphaboradibenzofulvene, these results suggested the Al–P single-bond character and the clear separation of the Lewis acid and Lewis base moieties due to the slight interaction between Al and P in **1**.



Scheme 3. (a) Reaction of the λ^3, λ^3 -phosphanylalumane **1** with benzophenone. (b) Reaction of the phosphaboradibenzofulvene with benzophenone, reported by Lerner et al.

3. Materials and Methods

3.1. General

All the manipulations were performed under a dry argon atmosphere using standard Schlenk techniques or gloveboxes. Solvents were purified by the Ultimate Solvent System, Glass Contour Company (Nikko Hansen and Co., Ltd., Osaka, Japan) (THF, toluene, and *n*-hexane) [29] or by trap-to-trap distillation from a potassium mirror prior to use (C_6D_6 and *n*-hexane for UV-vis spectrum measurements). NMR spectra were measured on a JMM-ECA600 (JEOL Ltd., Tokyo, Japan) (^1H : 600 MHz, ^7Li : 233 Hz, ^{13}C : 151 MHz, ^{19}F : 565 MHz, ^{27}Al : 156 MHz, ^{31}P : 243 MHz) in the Joint Usage/Research Center (JURC, Institute for Chemical Research, Kyoto University) or on a AL-300 spectrometer (JEOL Ltd., Tokyo, Japan) (^1H : 300 MHz, ^{13}C : 75 MHz, ^{19}F : 282 MHz, ^{31}P : 121 MHz). Regarding the ^1H NMR spectra, signals arising from residual partially hydrogenated $\text{C}_6\text{D}_5\text{H}$ (7.15 ppm for ^1H) were used as references. C_6D_6 (128.0 ppm for ^{13}C) and $\text{Al}(\text{NO}_3)_3$ in D_2O (0 ppm for ^{27}Al) were used as references. ^1H and ^{13}C NMR signals were assigned with the aid of the ^1H - ^1H COSY, ^1H - ^{13}C HSQC, and ^1H - ^{13}C HMBC spectra. Melting points were determined on a Yanaco micro melting point apparatus and uncorrected. Elemental analyses were carried out at the Microanalytical Laboratory, Institute for Chemical Research, Kyoto University.

AlCl_3 and AlBr_3 (Sigma-Aldrich Co., LLC., Tokyo, Japan), to prepare aluminum reagents, were purified by sublimation prior to use. The aluminum monohalides ($(t\text{-Bu})_2\text{AlBr}$ [21], and $(\text{C}_6\text{F}_5)_2\text{AlX}$ (X = Cl, Br) or $(\text{C}_6\text{F}_5)_2\text{AlCl} \cdot 0.5(\text{toluene})$ [23]) were prepared in accordance with the reported procedures. Mes_2PLi was prepared by the reaction of Mes_2PH with *n*-butyllithium in *n*-hexane, and the yellow solid was washed with *n*-hexane carefully to remove the residual Mes_2PH [22]. Details of theoretical calculations and XRD data are given in the Supplementary Materials.

3.2. Synthesis of **1**

To a yellow suspension of Mes_2PLi (277.2 mg, 1.00 mmol) in *n*-hexane (3 mL), $(t\text{-Bu})_2\text{AlBr}$ (219.5 mg, 0.998 mmol, 1.0 eq.) was slowly added at room temperature. The reaction mixture was stirred for 12 h. The almost quantitative formation of λ^3, λ^3 -phosphanylalumane was observed, as judged by ^{31}P NMR spectroscopy. The insoluble materials were removed by filtration through a Celite[®] pad using *n*-hexane as an eluent. The filtrate was concentrated and stored at -35°C , presenting λ^3, λ^3 -phosphanylalumane (**1**) as yellow crystals (isolated yield: 214.0 mg, 0.521 mmol, 52%). **1**: Yellow crystals, mp. $54\text{--}55^\circ\text{C}$. ^1H NMR (600 MHz, C_6D_6 , 298 K): $\delta = 1.09$ (d, 18H, $^4J_{\text{HP}} = 1.2$ Hz, $\text{C}(\text{CH}_3)_3$), 2.09 (s, 6H, Mes *p*- CH_3),

2.36 (s, 12H, Mes *o*-CH₃), 6.74 (m, 4H, Mes *m*-CH) ppm. ¹³C{¹H} NMR (151 MHz, C₆D₆, 298 K): δ = 20.9 (Mes *p*-CH₃), 24.5 (d, ³J_{CP} = 13.6 Hz, Mes *o*-CH₃), 29.7 (d, ³J_{CP} = 1.7 Hz, Al-C(CH₃)₃), 30.53 (s, AlCMe₃), 129.62 (d, ³J_{CP} = 3.0 Hz, Mes *m*-C), 133.79 (d, ²J_{CP} = 16.6 Hz, Mes *o*-C), 136.13 (s, Mes *p*-C), 141.19 (d, ¹J_{CP} = 12.1 Hz, Mes *ipso*-C) ppm. ²⁷Al NMR (156 MHz, C₆D₆, 298 K): δ = 261.3 (br.) ppm. ³¹P{¹H} NMR (243 MHz, C₆D₆, 298 K): δ = -111.7 ppm. UV-vis (hexane): λ/nm = 314 (ε 5.2 × 10³), 349 (ε 1.5 × 10³). Anal. Calcd. for C₂₆H₄₀AlP: C, 76.06; H, 9.82. Found: C, 76.07; H, 10.10.

3.3. Synthesis of **1**·(*t*-BuNC)

To a yellow solution of **1** (40.3 mg, 0.0982 mmol) in C₆D₆ (0.6 mL), a small excess amount of *t*-BuNC (9.6 mg, 0.115 mmol, 1.2 eq.) was slowly added at room temperature. The quantitative formation of **1**·(*t*-BuNC) was observed, as judged by ³¹P NMR spectroscopy. The mixture was concentrated at room temperature presenting the orange crystals. The crystals were washed with hexane to afford **1**·(*t*-BuNC) as light orange crystals (isolated yield: 16.4 mg, 0.0332 mmol, 34%). **1**·(*t*-BuNC): Light orange crystals, mp. 97–99 °C. ¹H NMR (600 MHz, C₆D₆, 298 K): δ = 0.64 (s, 9H, C≡N-C(CH₃)₃), 1.35 (d, ⁴J_{HP} = 0.6 Hz, 18H, AlC(CH₃)₃), 2.14 (s, 6H, Mes *p*-CH₃), 2.55 (s, 12H, Mes *o*-CH₃), 6.80 (m, 4H, Mes *m*-H) ppm. ¹³C{¹H} NMR (151 MHz, C₆D₆, 298 K): δ = 18.01 (d, ²J_{CP} = 12.1 Hz, AlCMe₃), 20.95 (s, Mes *p*-CH₃), 25.47 (d, ³J_{CP} = 10.6 Hz, Mes *o*-CH₃), 28.40 (s, C≡N-C(CH₃)₃), 32.56 (d, ³J_{CP} = 2.4 Hz, AlC(CH₃)₃), 57.72 (s, C≡NCMe₃), 129.04 (d, ³J_{CP} = 4.5 Hz, Mes *m*-C), 132.56 (d, ²J_{CP} = 33.2 Hz, Al←C≡N-*t*-Bu), 134.66 (s, Mes *p*-C), 137.19 (d, ²J_{CP} = 18.1 Hz, Mes *o*-C), 142.19 (d, ¹J_{CP} = 10.6 Hz, Mes *ipso*-C) ppm. ²⁷Al NMR (156 MHz, C₆D₆, 298 K): δ = +154.7 (br.) ppm. ³¹P{¹H} NMR (121 MHz, C₆D₆, 298 K): δ = -154 ppm. Anal. Calcd for C₃₁H₄₉AlNP: C, 75.42; H, 10.00; N, 2.84. Found: C, 75.02; H, 10.10; N, 2.83.

3.4. Synthesis of **2**·LiCl

To a yellow suspension of Mes₂PLi (25.4 mg, 0.0939 mmol) in *n*-hexane (2 mL), (C₆F₅)₂AlCl·0.5(toluene) (47.0 mg, 0.0942 mmol) was added at room temperature. The reaction mixture was stirred until the yellow color diminished (for 12 h). Following removal of the solvent, the residue was washed with the *n*-hexane. The insoluble materials were filtered through a Celite[®] pad using toluene as an eluent. *n*-Hexane was added to the filtrate and the mixture was scratched to give the colorless precipitate. The precipitate was washed with *n*-hexane carefully to afford (C₆F₅)₂Al-PMes₂·LiCl complex (**2**·LiCl) as a colorless solid (34.3 mg, 0.0510 mmol, 54%). **2**·LiCl: Colorless solid, mp. 94 °C (dec.). ¹H NMR (600 MHz, C₆D₆, 298 K): δ = 1.96 (s, 6H, Mes *p*-CH₃), 2.23 (s, 12H, Mes *o*-CH₃), 6.58 (d, ⁴J_{HP} = 2.4 Hz, 4H, Mes *m*-H) ppm. ⁷Li{¹H} NMR (233 MHz, C₆D₆, 298K): δ = -4.73 ppm. ¹³C{¹H} NMR (151 MHz, C₆D₆, 298K): δ = 20.70 (s, Mes *p*-CH₃), 24.75 (d, ³J_{CP} = 9.1 Hz, Mes *o*-CH₃), 117.05 (br. t, ²J_{CF} = ~49 Hz, C₆F₅ *ipso*-C), 133.21 (d, ²J_{CF} = 9.1 Hz, Mes *o*-C), 137.09 (s, Mes *p*-C), 137.26 (dq, ¹J_{CF} = 252 Hz, ²J_{CF} = ~12 Hz, ³J_{CF} = ~4.5 Hz, C₆F₅ *m*-C), 141.53 (dm, ¹J_{CF} = 252 Hz, C₆F₅ *p*-C), 143.13 (d, ¹J_{CP} = 10.6 Hz, Mes *ipso*-C), 149.94 (ddm, ¹J_{FC} = 224 Hz, ²J_{FC} = 24 Hz, C₆F₅ *o*-C) ppm. ¹⁹F NMR (282 MHz, C₆D₆, 298 K): δ = -123.3 (m, 4F, C₆F₅ *o*-F), -155.4 (t, J = 19.7 Hz, 2F, C₆F₅ *p*-F), -161.2 (m, 4F, C₆F₅ *m*-F) ppm. ³¹P{¹H} NMR (121 MHz, C₆D₆, 298 K): δ = -89.7 (br. s) ppm. No ²⁷Al NMR signal was observed, even after long-time measurement. Due to the flame retardancy of fluorocarbons and the extremely high air-/moisture-sensitivity, satisfactory data of the elemental analysis could not be obtained. The purity of **2**·LiCl was confirmed accordingly by the ¹⁹F and ³¹P{¹H} NMR spectra.

3.5. Synthesis of **2**·LiBr

To a yellow suspension of Mes₂PLi (11.9 mg, 0.044 mmol) in *n*-hexane (2 mL), (C₆F₅)₂AlBr (23.3 mg, 0.0441 mmol) was added at room temperature. The solution was stirred until the yellow color diminished (for 5 h). The precipitate was washed with the *n*-hexane, and the residue was filtered through a Celite[®] pad using toluene as an eluent. Following removal of the solvent from the filtrate, the resulting materials (14.5 mg) was checked by NMR spectroscopy, suggesting the formation of

(C₆F₅)₂Al–PMes₂–LiBr complex (**2·LiBr**). Further purification and isolation did not succeed. **2·LiBr**: A colorless solid of crude materials. ¹H NMR (300 MHz, C₆D₆, 298 K): δ = 1.96 (s, 6H, Mes *p*-CH₃), 2.22 (s, 12H, Mes *o*-CH₃), 6.59 (m, 4H, Mes *m*-H) ppm. ⁷Li{¹H} NMR (117 MHz, C₆D₆, 298 K): δ = −4.38 ppm. ¹⁹F NMR (282 MHz, C₆D₆, 298 K): δ = −122.9 (m, 4F, C₆F₅ *o*-F), −152.9 (t, *J* = 19.7 Hz, 2F, C₆F₅ *p*-F), −160.8 (m, 4F, C₆F₅ *m*-F) ppm. ³¹P{¹H} NMR (121 MHz, C₆D₆, r.t.): δ = −89.3 (s) ppm.

3.6. Synthesis of **2·Et₂O**

To a yellow suspension of Mes₂PLi (24.2 mg, 0.0485 mmol) in Et₂O (2 mL), (C₆F₅)₂AlCl·0.5(toluene) (13.3 mg, 0.0492 mmol) was added at room temperature. Following removal of the solvent immediately, the residue was washed with *n*-hexane. The insoluble materials were separated by filtration through a Celite® pad using toluene as an eluent. Subsequent to removal of the solvent from the filtrate, the residue was washed several times with *n*-hexane to afford (C₆F₅)₂Al–PMes₂·Et₂O (**2·Et₂O**) as a colorless solid (14.3 mg, 0.0203 mmol, 38%). Colorless crystals, mp. 129 °C (dec.). ¹H NMR (300 MHz, C₆D₆, 298 K): δ = 0.35 (t, 6H, OCH₂CH₃), 2.09 (s, 6H, Mes *p*-CH₃), 2.35 (s, 12H, Mes *o*-CH₃), 3.76 (q, 4H, OCH₂CH₃), 6.74 (m, 4H, Mes *m*-H). ¹⁹F NMR (282 MHz, C₆D₆, 298 K): δ = −119.4 (m, 4F, C₆F₅ *o*-F), −152.5 (t, *J* = 19.7 Hz, 2F, C₆F₅ *p*-F), −161.1 (m, 4F, C₆F₅ *m*-F) ppm. ³¹P{¹H} NMR (121 MHz, C₆D₆, r.t.): δ = −104.8 ppm. No ²⁷Al NMR signal was observed, even after long-time measurement. Satisfactory data of the ¹³C NMR spectrum could not be obtained due to the impurities and decomposition. Due to the flame retardancy of fluorocarbons and the extremely high air-/moisture-sensitivity, satisfactory data of the elemental analysis could not be obtained.

3.7. Reaction of **2·LiCl** with Et₂O

The solid of **2·LiCl** (1.2 mg, 0.0018 mmol) was slowly dissolved Et₂O (1 mL) at room temperature. The solvent was removed immediately and the mixture was analyzed by ¹H and ¹⁹F NMR spectroscopy, presenting a mixture the same as the observation of the reaction for the (C₆F₅)₂AlCl with Mes₂PLi in Et₂O solution. This result indicated that **2·LiCl** is formed at the initial stage of the reaction and Et₂O is coordinated toward **2·LiCl** or promotes decomposition of **2·LiCl**.

3.8. Thermal Isomerization of **1·(t-BuNC)**

Using a J.Young NMR tube, a solution of **1·(t-BuNC)** (5.6 mg, 0.011 mmol) in C₆D₆ (0.6 mL) was degassed by freeze-pump-thaw cycles and heated at 100 °C over 48 h. The signals of the corresponding **1**, **1·(t-BuNC)**, Mes₂PH, Mes₂P–PMes₂ were observed by ³¹P{¹H} NMR spectroscopy. The recrystallization from a mixture afforded a trace amount of **3** as red crystals.

3.9. Reaction of **1** with Benzophenone

Using a J.Young NMR tube, a solution of **1** (12.7 mg, 0.0309 mmol) in C₆D₆ (0.6 mL) was treated with an excess amount of benzophenone (9.2 mg, 0.0505 mmol, 1.6 eq.) at room temperature. The quantitative formation of Mes₂P–PMes₂ was observed, as judged by ³¹P{¹H} NMR spectroscopy.

3.10. X-Ray Crystallographic Analysis

The intensity data were collected on a Saturn 70 CCD diffractometer (Rigaku Corp., Tokyo, Japan) with a VariMax Mo optic system using Mo K α radiation (λ = 0.71075 Å) [for **1**, **1·(t-BuNC)**, and **2·LiCl**], or a Mercury CCD diffractometer (Rigaku Corp., Tokyo, Japan) with graphite monochromated Mo K α radiation (λ = 0.71069 Å) (for **2·Et₂O**). An empirical absorption correction was applied to the diffraction data using ABSPACK [30] for **1**, **1·(t-BuNC)**, **2·LiCl**, and **2·Et₂O**. The structure was solved by a direct method (SHELXT [31]) and refined by a full-matrix least-squares method on *F*² for all reflections (SHELXL-2016/4 [32]). All hydrogen atoms were placed using AFIX instructions, while all other atoms were refined anisotropically. CCDC-1959322 (**1**), CCDC-1959323 [**1·(t-BuNC)**], CCDC-1959324 (**2·Et₂O**), and CCDC-1959325 (**2·LiCl**) contain the supplementary crystallographic data for this paper.

These data can be obtained free of charge from The Cambridge Crystallographic Data Centre via www.ccdc.cam.ac.uk/data_request/cif.

3.11. Theoretical Calculations

DFT calculations were performed using the Gaussian 16 (Rev. B. 01) [33] program package (Gaussian, Inc., Wallingford, CT, USA) with B3LYP functional [34–36] including Grimme dispersion correction (D3) [37,38] along with a combined basis set: 6-31G(d) level. All the geometry optimizations were performed until the residual mean force was smaller than 1.0×10^{-5} a.u. (*tight* threshold in Gaussian). The frequency calculations were carried out for each optimized structure to confirm the absence of any imaginary frequencies. The vertical excitation energy and electronic absorption spectra were simulated using time-dependent density functional theory (TD-DFT) [39] at the B3LYP-D3/6-311G+(d,p)//B3LYP-D3/6-31G(d) level. Natural bond orbital (NBO) analyses were conducted with the NBO 6.0 program package [40], linked to single-point calculations using Gaussian 16 (Rev. B. 01)

4. Conclusions

To summarize, we reported here the synthesis and structures of novel phosphanylalumane derivatives whose protecting groups on the Al and P atoms are all carbon substituents. Substituent effects on an Al atom were investigated, and the introduction of C_6F_5 groups on the Al atom substantially increased the Lewis acidity of aluminum. Additionally, they presented extremely short Al–P bond lengths compared to those of related compounds. Based on the results of X-ray crystallographic analysis, theoretical calculations, and the reaction with benzophenone, λ^3, λ^3 -phosphanylalumane **1** was found to have a well-separated vacant p orbital on an Al atom and lone pairs on a P atom. Its spectroscopic properties were investigated for the first time, presenting a yellow color due to the charge transfer character between Al and P atoms in λ^3, λ^3 -phosphanylalumane. Further studies on the reactivity of phosphanylalumanes are now under way.

Supplementary Materials: The following are available online at <http://www.mdpi.com/2304-6740/7/11/132/s1>. NMR spectra. Crystallographic data (CCDC 1959322–1959325) and theoretical calculations details. Supplementary material includes the CIF and CheckCIF files for **1**, **1-(t-BuNC)**, **2-LiCl**, and **2-Et₂O**.

Author Contributions: T.Y. designed the project and performed the experiments and measurements. T.Y. carried out the X-ray crystallographic analysis and theoretical calculations. T.Y. and Y.M. designed the experiments. T.Y. and Y.M. co-wrote the paper. T.Y., Y.M., and N.T. reviewed and approved the final manuscript. All authors contributed to the discussions.

Funding: This research was partially funded by JSPS KAKENHI (JP24109013 and JP26620028), JSPS Research Fellowship for Young Scientists (JP19J14359), and Integrated Research Consortium on Chemical Science (IRCCS).

Acknowledgments: This study was supported by the Joint Usage/Research Center [JURC, Institute for Chemical Research (ICR), Kyoto University] by providing access to a JEOL JNM-ECA600 NMR spectrometer. The authors are furthermore grateful for computation time, which was provided by the Super Computer System (ICR, Kyoto University). Elemental analyses were carried out at the Microanalytical Laboratory of the ICR (Kyoto University).

Conflicts of Interest: The authors declare no conflict of interest.

References

1. Niedenzu, K.; Dawson, J.W. Aminoboranes. In *Boron-Nitrogen Compounds*; Niedenzu, K., Dawson, J.W., Eds.; Springer: Berlin/Heidelberg, Germany, 1965; pp. 48–84.
2. Bullen, G.J.; Clark, N.H. Crystallographic studies of the boron–nitrogen bond in aminoboranes. Part II. Crystal structure of (dimethylamino) dimethylborane at -95°C . *J. Chem. Soc. A* **1970**, 992–996. [[CrossRef](#)]
3. Brauer, D.J.; Bier, H.; Diirrenbach, F.; Pawelke, G.; Weuter, W. Synthesis of diethyl- and diisopropylamino-trifluoromethylboranes and their reactions with HF, HCl, HBr and H₂O. The crystal structure of $(\text{CF}_3)_2\text{BN}(i\text{-Pr})_2$, revealing a very short B–N bond. *J. Organomet. Chem.* **1989**, 378, 125–137. [[CrossRef](#)]

4. Faderl, J.; Deobald, B.; Guillard, R.; Pritzkow, H.; Siebert, W. Syntheses, structures, and reactivity of 2,5-diboryl-1-alkylpyrroles and di(1-alkyl-2-pyrrolyl)boranes. *Eur. J. Inorg. Chem.* **1999**, 1999, 399–404. [[CrossRef](#)]
5. Paine, R.T.; Nöth, H. Recent advances in phosphinoborane chemistry. *Chem. Rev.* **1995**, 95, 343–349. [[CrossRef](#)]
6. Bailey, J.A.; Pringle, P.G. Monomeric phosphinoboranes. *Coord. Chem. Rev.* **2015**, 297–298, 77–90. [[CrossRef](#)]
7. Stephan, D.W. Frustrated Lewis Pairs. *J. Am. Chem. Soc.* **2015**, 137, 10018–10032. [[CrossRef](#)]
8. Stephan, D.W.; Erker, G. Frustrated Lewis Pair Chemistry: Development and Perspectives. *Angew. Chem. Int. Ed.* **2015**, 54, 6400–6441.
9. Stephan, D.W. The broadening reach of frustrated Lewis pair chemistry. *Science* **2016**, 354, aaf7229. [[CrossRef](#)]
10. Jupp, A.R.; Stephan, D.W. New Directions for Frustrated Lewis Pair Chemistry. *Trends Chem.* **2019**, 1, 35–48. [[CrossRef](#)]
11. Atwood, D.A.; Contreras, L.; Cowley, A.H.; Jones, R.A.; Mardones, M.A. Monomeric base-stabilized phosphino- and arsinoalanes. *Organometallics* **1993**, 12, 17–18. [[CrossRef](#)]
12. Petrie, M.A.; Power, P.P. Synthesis and characterization of the monomeric phosphinogallanes $\text{Bu}^t_2\text{GaPR}''$ (R' , R'' = bulky aryl or silyl groups) and related compounds. *J. Chem. Soc. Dalton Trans.* **1993**, 1737–1745. [[CrossRef](#)]
13. Agou, T.; Ikeda, S.; Sasamori, T.; Tokitoh, N. Synthesis and structure of Lewis base-coordinated phosphanylalumanes bearing P–H and Al–Br moieties. *Eur. J. Inorg. Chem.* **2018**, 2018, 1984–1987. [[CrossRef](#)]
14. Wehmschulte, R.J.; Ruhlandt-Senge, K.; Power, P.P. Synthesis and characterization of unassociated aluminum monophosphides. *Inorg. Chem.* **1994**, 33, 3205–3207. [[CrossRef](#)]
15. Knabel, K.; Krossing, I.; Nöth, H.; Schwenk-Kircher, H.; Schmidt-Amelunxen, M.; Seifert, T. The aluminum–nitrogen bond in monomeric bis(amino)alanes: A systematic experimental study of bis(tetramethylpiperidino)alanes and quantum mechanical calculations on the model system $(\text{H}_2\text{N})_2\text{AlY}$. *Eur. J. Inorg. Chem.* **1998**, 1998, 1095–1114. [[CrossRef](#)]
16. Haberer, T.; Nöth, H.; Paine, R.T. Synthesis and reactivity of new bis(tetramethylpiperidino)(phosphanyl)alumanes. *Eur. J. Inorg. Chem.* **2007**, 2007, 4298–4305. [[CrossRef](#)]
17. Agou, T.; Ikeda, S.; Sasamori, T.; Tokitoh, N. Synthesis and structure of Lewis-base-free phosphinoalumane derivatives. *Eur. J. Inorg. Chem.* **2016**, 2016, 623–627. [[CrossRef](#)]
18. Wehmschulte, R.J.; Power, P.P. Reactions of $(\text{H}_2\text{AlMes}^*)_2$ ($\text{Mes}^* = 2,4,6\text{-}(t\text{-Bu})_3\text{C}_6\text{H}_2$) with H_2EAr ($\text{E} = \text{N}, \text{P}$, or As ; $\text{Ar} = \text{aryl}$): Characterization of the ring compounds $(\text{Mes}^*\text{AlNPh})_2$ and $(\text{Mes}^*\text{AlEPh})_3$ ($\text{E} = \text{P}$ or As). *J. Am. Chem. Soc.* **1996**, 118, 791–797. [[CrossRef](#)]
19. Agou, T.; Yanagisawa, T.; Sasamori, T.; Tokitoh, N. Synthesis and structure of an iron-bromoalumanyl complex with a tri-coordinated aluminum center. *Bull. Chem. Soc. Jpn.* **2016**, 89, 1184–1186. [[CrossRef](#)]
20. Yanagisawa, T.; Mizuhata, Y.; Tokitoh, N. Dibromometallyl-iron complexes generated by the recombination of an alumanyl-iron complex with EBr_3 ($\text{E} = \text{Al}, \text{Ga}$). *Heteroatom Chem.* **2018**, 29, e21465. [[CrossRef](#)]
21. Uhl, W.; Schnepf, J.E.O.Z. Synthesis and molecular structure of $(N,N'$ -dimethylpiperazine)lithium- μ -hydrido(*tert*-butyl)bis[bis(trimethylsilyl)methyl]alanate with an intramolecular interaction between lithium and C–H- σ -bonds. *Z. Anorg. Allg. Chem.* **1991**, 595, 225–238. [[CrossRef](#)]
22. Geier, S.J.; Gilbert, T.M.; Stephan, D.W. Synthesis and reactivity of the phosphinoboranes $\text{R}_2\text{PB}(\text{C}_6\text{F}_5)_2$. *Inorg. Chem.* **2011**, 50, 336–344. [[CrossRef](#)]
23. Styra, S.; Radius, M.; Moos, E.; Bihlmeier, A.; Breher, F. Aluminium diphosphamethanides: Hidden frustrated Lewis pairs. *Chem. Eur. J.* **2016**, 22, 9508–9512. [[CrossRef](#)]
24. Uhl, W.; Schütz, U.; Hillerb, W.; Heckell, M. Reaction of isothiocyanates and isonitriles with $\text{R}_2\text{Al}-\text{AlR}_2$ [$\text{R} = \text{CH}(\text{SiMe}_3)_2$]; single and double insertion of isonitrile into the Al–Al bond. *Chem. Ber.* **1994**, 127, 1587–1592. [[CrossRef](#)]
25. Nagata, K.; Agou, T.; Sasamori, T.; Tokitoh, N. Formation of a diaminoalkyne derivative by dialumane-mediated homocoupling of *t*-butyl isocyanide. *Chem. Lett.* **2015**, 44, 1610–1612. [[CrossRef](#)]
26. Chen, W.; Zhao, Y.; Xu, W.; Su, J.-H.; Shen, L.; Liu, L.; Wu, B.; Yang, X.-J. Reductive linear- and cyclo-trimerization of isocyanides using an Al–Al-bonded compound. *Chem. Commun.* **2019**, 55, 9452–9455. [[CrossRef](#)]

27. Knabel, K.; Nöth, H. Synthesis and structures of some aluminum pseudohalides. *Z. Naturforsch.* **2005**, *60b*, 155–163. [[CrossRef](#)]
28. Breunig, J.M.; Hübner, A.; Bolte, M.; Wagner, M.; Lerner, H.-W. Reactivity of phosphoradibenzofulvene toward hydrogen, acetonitrile, benzophenone, and 2,3-dimethylbutadiene. *Organometallics* **2013**, *32*, 6792–6799. [[CrossRef](#)]
29. Pangborn, A.B.; Giardello, M.A.; Grubbs, R.H.; Rosen, R.K. Silicon carbon unsaturated compounds. 21. Isomerization of a 1-silapropadiene in the presence of tetrakis(triethylphosphine)nickel(0). *Organometallics* **1996**, *5*, 1518–1520. [[CrossRef](#)]
30. CrysAlis, C.C.D. *CrysAlis RED including ABSPACK, Versions 1.171.39.46*; Oxford Diffraction Ltd.: Abingdon, UK, 2006.
31. Sheldrick, G.M. SHELXT—Integrated space-group and crystal-structure determination. *Acta Crystallogr. Sect. A* **2015**, *71*, 3–8. [[CrossRef](#)]
32. Sheldrick, G.M. Crystal structure refinement with SHELXL. *Acta Crystallogr. Sect. C* **2015**, *71*, 3–8. [[CrossRef](#)]
33. Frisch, M.J.; Trucks, G.W.; Schlegel, H.B.; Scuseria, G.E.; Robb, M.A.; Cheeseman, J.R.; Scalmani, G.; Barone, V.; Petersson, G.A.; Li, X.; et al. *Gaussian 16, Revision B.01*; Gaussian, Inc.: Wallingford, CT, USA, 2016.
34. Becke, A.D. Density-functional thermochemistry. III. The role of exact exchange. *J. Chem. Phys.* **1993**, *98*, 5648–5662. [[CrossRef](#)]
35. Becke, A.D. Density-functional exchange-energy approximation with correct asymptotic behavior. *Phys. Rev. A* **1988**, *38*, 3098–3100. [[CrossRef](#)] [[PubMed](#)]
36. Lee, C.; Yang, W.; Parr, R.G. Development of the Colle-Salvetti correlation-energy formula into a functional of the electron density. *Phys. Rev. B* **1988**, *37*, 785–789. [[CrossRef](#)] [[PubMed](#)]
37. Grimme, S.; Antony, J.; Ehrlich, S.; Krieg, H. A consistent and accurate ab initio parametrization of density functional dispersion correction (DFT-D) for the 94 elements H-Pu. *J. Chem. Phys.* **2010**, *132*, 154104–154119. [[CrossRef](#)]
38. Grimme, S.; Ehrlich, S.; Goerigk, L. Effect of the damping function in dispersion corrected density functional theory. *J. Comput. Chem.* **2011**, *32*, 1456–1465. [[CrossRef](#)]
39. Runge, E.; Gross, E.K.U. Density-functional theory for time-dependent systems. *Phys. Rev. Lett.* **1984**, *52*, 997–1000. [[CrossRef](#)]
40. Glendening, E.D.; Badenhoop, J.K.; Reed, A.E.; Carpenter, J.E.; Bohmann, J.A.; Morales, C.M.; Landis, C.R.; Weinhold, F. *NBO 6.0*; Theoretical Chemistry Institute, University of Wisconsin: Madison, WI, USA, 2013.



© 2019 by the authors. Licensee MDPI, Basel, Switzerland. This article is an open access article distributed under the terms and conditions of the Creative Commons Attribution (CC BY) license (<http://creativecommons.org/licenses/by/4.0/>).